Journal of Materials Chemistry A

ROYAL SOCIETY OF CHEMISTRY

PAPER

View Article Online
View Journal | View Issue

Cite this: J. Mater. Chem. A, 2024, 12, 7826

Meta-kinks are key to binder performance of poly(arylene piperidinium) ionomers for alkaline membrane water electrolysis using non-noble metal catalysts†

Richard Weber,[a] Malte Klingenhof,[b] Susanne Koch,[cd] Lukas Metzler,[cd] Thomas Merzdorf,[b] Jochen Meier-Haack,[e] Peter Strasser,[b] Severin Vierrath[cd] and Michael Sommer*[af]

Anion-exchange membrane water electrolysis (AEMWE) is a key technology for the production of green hydrogen at high current densities without the necessity of noble metal catalysts. AEMWE technology does not only rely on chemically stable and highly hydroxide-conducting membranes, but also on ionomer binders, to which additional criteria apply related to swelling, mechanical properties, gas permeability and porosity to form a triple phase boundary with catalyst particles on top of an membrane electrode assembly (MEA). Here, we investigate seven poly(arylene piperidinium)s (PAPs) with different ratios of *meta*-/*para*-terphenyl building blocks as binders for non-noble NiFe-LDH catalysts. We first analyze the materials comprehensively in pristine form and subsequently as binders. With increasing content of *meta*-terphenyl, specific surface area, water uptake, swelling ratio and ion-conductivity increase continuously, with the latter ranging from 145 to 216 mS cm^{-1} at 80 °C. We elucidate binder performance from rotating disk electrode experiments of oxygen evolution reactions (OER) catalysed by nickel–iron layered double hydroxides (NiFe-LDH) under AEMWE working potentials. Here, an increasing content of *meta*-kinks leads to improved catalyst utilization, superior OER performance and improved electrode stability. Finally, AEMWE single cell tests show a strong improvement in current density when altering binders from exclusively *para*- to *meta*-terphenyl in the polymer backbone. Current densities as high as 1000 to 1700 mA cm^{-2} at 1.8 V and 3000 mA cm^{-2} at 2.0 V are measured for the binder with exclusive *meta*-terphenyl kinks. The results highlight the role of the binder for AEMWE performance as well as the importance of its individual optimization aside from membrane properties.

Received 10th November 2023
Accepted 15th February 2024

DOI: 10.1039/d3ta06916h

rsc.li/materials-a

Introduction

Green hydrogen production using water electrolysis is a key technology for future industrial decarbonization as well as establishing an economy with climate-friendly energy storage and supply.[1,2] Since conventional alkaline water electrolysers are limited in the achievable current density, the zero-gap configuration in polymer electrolyte water electrolysis is highly favourable for effective hydrogen production.[1] Although proton-exchange membrane water electrolysis is widely studied and meanwhile established, the inevitable use of expensive precious metal electrocatalysts like platinum or iridium makes this technique less cost-effective. In contrast, anion-exchange membrane water electrolysers (AEMWE) combine the advantages of alkaline water electrolysis and proton-exchange membrane water electrolysis, as abundant non-precious metal catalysts can be used and operation at high current density can be achieved.[3,4]

The central component of AEMWE is the membrane electrode assembly (MEA). The two main MEA designs are catalyst coated substrates (CCS) and catalyst coated membranes (CCM).[5] For CCS, the porous transport layers are covered with a catalyst or activated by growing catalysts on their surfaces.[6,7] A CCM for AEMWE consists of an anion-exchange membrane (AEM)

[a]Institute for Chemistry, Chemnitz University of Technology, Straße der Nationen 62, 09111 Chemnitz, Germany. E-mail: michael.sommer@chemie.tu-chemnitz.de
[b]Department of Chemistry, Technical University Berlin, Straße des 17. Juni 124, 10623 Berlin, Germany. E-mail: pstrasser@tu-berlin.de
[c]Electrochemical Energy Systems, IMTEK-Department of Microsystems Engineering, University of Freiburg, Georges-Koehler-Allee 103, 79110 Freiburg, Germany. E-mail: severin.vierrath@imtek.uni-freiburg.de
[d]Hahn-Schickard, Georges-Koehler-Allee 103, 79110 Freiburg, Germany
[e]Leibniz-Institut für Polymerforschung Dresden e.V., Hohe Straße 6, 01069 Dresden, Germany
[f]Research Center for Materials, Architectures and Integration of Nanomembranes (MAIN), Chemnitz University of Technology, Straße der Nationen 62, 09126 Chemnitz, Germany

† Electronic supplementary information (ESI) available. See DOI: https://doi.org/10.1039/d3ta06916h

coated on both sides with a mixture of catalysts for anodic and cathodic reactions and ion-conducting binder polymer. The membrane separates the half cells, conducts hydroxide ions and catalyses water electrolysis. As the electrochemical reactions take place at the surface of the catalyst particles, an optimal contact between membrane, binder, catalyst and conductive carbon is required.[8–10] The CCM approach typically leads to lower ohmic resistance compared to the CCS approach and consequently to higher cell performances.[5] To achieve an optimal morphology with a so-called triple-phase-boundary involving the solid catalyst, the polymeric hydroxide conductor and the gaseous products, the properties of the binder ionomer are considered key for long-term stability of the MEA.[8,11,12] Mechanical properties, interaction with catalyst, ionic conductivity, water uptake and swelling all play a role.[8,12,13] In addition, gas permeability is important as insufficient gas removal limits mass transport and finally performance of the electrolyser.[10,12,13] In addition to these aspects, binder properties need to be adjusted to allow processing dispersions of catalyst particles in the mixtures used for membrane coating or catalyst layer fabrication.[8,11–15] The latter is crucial for homogeneous distribution of catalyst particles, maximised electrochemically active surface and effective transport of reactants and products.[11,13]

Progress in AEM materials is impressive,[16–18] yet studies that explicitly address the role of the binder and its optimization are much less prevalent.[15,19,20] Different binder ionomers based on polyethylene,[21,22] polystyrene,[19,23] polysulfones,[24–27] polyphenylene oxides,[28,29] polybenzimidazoles[30,31] or poly(arylene alkylene)s[15,20,32] have been used. Beside these, also Nafion[33,34] and polytetrafluoroethylene[34–36] have been reported.

One prominent class of polymers for AEM applications are rigid, aromatic polymers prepared *via* superacid-catalysed polyhydroxyalkylation. The synthetic simplicity, commercial availability of arylene monomers and chemical stability make poly(arylene alkylene)s highly attractive. As a result, a variety of poly(arylene alkylene)s has been prepared, including poly-(arylene alkylene)s,[37–40] poly(arylene isatine)s,[41–43] poly(xanthene)s[44,45] or poly(arylene piperidinium)s.[40,46–49] Among them, poly(arylene piperidinium)s are most comprehensively studied as main-chain anion-exchange polymers. The starting materials involve 4-piperidone derivatives and diverse arylenes, most often *meta*-[40,50–53] or *para*-terphenyl.[32,40,46,48] Additionally, the influence of differently configurated backbone structures of poly(arylene alkylene)s and poly(arylene piperidinium)s on properties has been studied using *meta*- or *para*-terphenyl as arene building blocks. It was found that the incorporation of exclusively *meta*-terphenyl and the resulting kinked backbone structure promotes self-assembly and aggregation of cationic units, leading to improved hydration and increased conductivities compared to *para*-terphenyl analogs.[38] Partial substitution of *para*-terphenyl units in poly(*p*-terphenyl piperidinium)s with rigid dimethylfluorene has been further suggested to increase the free volume leading to increased hydration numbers and hydroxide conductivities.[54]

Despite this evidence of backbone constitution being a primary factor for packing density and porosity, the aforementioned works have focused on improving AEM properties. Detailed studies on the optimization of binder properties are lacking, despite accumulating evidence that this component of the MEA is central to performance and durability of AEMWE.[11,13,18] Binder ionomers must meet criteria of high dimensional and alkaline stability under aqueous and caustic conditions in order to gain long term stability of the MEA and the electrolysis cell. Detachment of catalyst particles due to chemical degradation or mechanical failure of binder materials is one main cause of AEMWE performance loss.[18] With respect to chemical stability under alkaline conditions, ether-linkage free backbone structures[17,55–60] functionalized with piperidiniums as anion-bearing moiety are beneficial. Wang *et al.* reported for a poly(arylene piperidinium) only 3% ionic loss after 2000 h immersion in 1 M KOH solution at 100 °C.[48] A similar polymer structure investigated by Olsson *et al.* exhibited merely 5% degradation after 360 h in 2 M KOH solution at 90 °C.[46] In addition, taking an AEMWE study by Lindquist *et al.* into account the commercial poly(arylene piperidinium) PiperION as binder and membrane material outperformed polybenzimidazole and polystyrene based ionomers.[15]

Herein we present a comprehensive study of the influence of backbone constitution of poly(terphenylene piperidinium)s with varying *meta*-terphenyl content on pristine as well as binder properties. Seven different statistical quaterpolymers are prepared with varying *meta*-/*para*- ratio, and their mechanical properties, swelling and ionic conductivity are investigated. Specific surface area, water uptake and swelling and ionic conductivity continuously increase with increasing *meta*-kink content. The prepared ionomers are excellent binders for nickel–iron layered double hydroxides (NiFe-LDH) catalysts, as probed by rotating disk electrode (RDE) experiments. Here, an increasing *meta*-kink content improves catalyst utilization and electrode stability. In AEMWE single cell tests an outstanding current density of 3000 mA cm^{-2} at 2 V is achieved with NiFe-LDH as catalyst and the binder with exclusive *meta*-terphenyl kinks.

Experimental

Details on polymer synthesis, materials and all other methods and experimental procedures are found in the ESI.†

Rotating disk electrode (RDE) experiments

For electrocatalytic activity testing with rotating disk electrode (RDE), a NiFe-LDH suspension was prepared from 4 mg NiFe-LDH, 768 μL de-ionised water, 200 μL *i*-propanol and 32 μL 5 wt% binder solution. 10 μL of the resulting dispersion was pipetted on the glassy carbon electrode. Electrocatalytic performance was evaluated in N_2-saturated 0.1 M KOH at 1600 rpm using a Biologic SP-200 potentiostat operating in a three-electrode setup with a platinum counter electrode (CE) and a reversible hydrogen (RHE) reference electrode, see also Tables S1, S2 and Fig. S1.† Reported CVs for evaluation of the electrochemical activity were *iR*- and capacity-corrected. The reported overpotentials necessary to reach a current density of

10 mA cm^{-2} (OER) are the average of three measurements. Stability measurements of the multi-component system were conducted with the same setup. Here, cycling experiments with 2000 CVs between 1.23 V *vs.* RHE and 1.63 V *vs.* RHE were conducted to periodically evaluate the OER performance.

Preparation of anode inks for bar coating

NiFe-LDH (400 mg) was dispersed in a mixture of i-propanol (IPA) and water (2.0 g, 1 : 1). After addition of the previously prepared ionomer solution (0.6 g, 5 wt% PAP in DMSO), ZrO_2 grinding balls (Retsch 22.455.0009) were added. After 2 days on a roll mixer (IKA, Roller 10) the inks were used for electrode fabrication *via* bar coating. In some cases, additional solvents (*e.g.* 200 μL IPA : water) had to be added on the day of cell fabrication to make the ink processable.

Preparation of cathode inks for bar coating

Pt/C 50 wt% (300 mg, Umicore Elyst Pt50 0550) was dispersed in water (1.8 g). After adding the previously prepared ionomer solution (1.8 g, 2.5 wt% Aemion$^+$-HNN8 in MeOH/H_2O 10/1), ZrO_2 grinding balls were added. After 2 days on a roll mixer the inks were used for electrode fabrication *via* direct bar coating.

Preparation of catalyst-coated membranes (CCMs)[61]

A membrane (Aemion$^+$, AP2-HNN8-50-X) was attached to a clean glass surface and the anode ink was carefully distributed with a bar coater (Thierry, PG-032-150200). After drying, the half-CCM was covered with an adhesive foil, while a PTFE foil protected the electrode layer. The backing foil was removed and the half-CCM was attached to the glass surface with the uncoated side facing up. The cathode ink was evenly distributed on the membrane with the help of the bar coater and dried over night. The catalyst loadings were measured by X-ray fluorescence microscope (μXRF, Bruker, M4 Tornado): the combined anode-loading of Ni and Fe for the M0 cell was 1.05 mg cm^{-2} and 0.97 mg cm^{-2} for the M100 cell. The average Pt-loading on the cathodes was 0.54 mg cm^{-2} for the M0 cell and 0.45 mg cm^{-2} for the M100 cell.

AEMWE single cell measurements

Single cell measurements were performed according to previously published work by Koch & Metzler *et al.* unless otherwise noted.[61] Briefly, MEAs were immersed in 3 M KOH for 24 h and subsequently immersed in 1 M KOH for another 24 h to perform ion-exchange to the hydroxide form. Nickel felt (200 μm, Bekaert) and carbon paper (H24C5, Freudenberg) were used as transport layers on the anode and cathode side, respectively. Using a custom-built cell fixture and AEMWE test bench, the MEAs were measured at 60 °C in 1 M KOH.[62] The electrolyte flow rate was set to 40 ml min^{-1} using a peristaltic pump and the electrolyte was pre-heated to 67 °C using a bath thermostat. A BioLogic VSP-300 potentiostat with two 10 A/5 V boosters was employed to measure polarization curves *via* electrochemical impedance spectroscopy to extract the high-frequency resistance (HFR).

Results and discussion

Polymer synthesis and characterization

The investigated binder polymers were synthesized by superacid-catalysed Friedel–Crafts-type polyhydroxyalkylation reaction and subsequent quaternization with methyl iodide according to literature.[48,63] The ratio of the electron-rich arene monomers *meta*-terphenyl (*m*-TP) and *para*-terphenyl (*p*-TP) was varied. The ratio of the ketone monomers 2,2,2-trifluoroacetophenone (TFAp) and 4-piperidone monohydrate hydrochloride (Pip) was set at 15 to 85 for each polymerization (Scheme 1) as previously reported.[48] Poly(arylene piperidinium)s are denoted as M*x*, where *x* is the percentage of *m*-TP in the feed (Table 1). The commercially available material PiperION by Versogen most closely resembles the M0 polymer synthesized herein. The successful incorporation of the monomers was confirmed by ^{1}H NMR spectroscopy (Fig. S2†). Due to the overlapping of the proton signals in the aromatic region, quantitatively distinguishing between *m*-TP and *p*-TP was not possible, however a qualitative evaluation of the signals in the aromatic region hints at the successful introduction of the different arenes according to their feed ratio (Fig. S3†). Molar masses and molar mass distributions were evaluated by size exclusion chromatography (SEC) in *N*,*N*-dimethylformamide (DMF) as eluent (Table 1 and Fig. S4†). In general, high molecular weight polymers with weight average molecular weights M_w > 50 kDa were obtained suitable for preparing mechanically stable films for further characterization.

Water uptake and swelling ratio

In AEMWEs the ionomeric binder is responsible for the transport of reactants (hydroxide ions and water) to the catalyst, as well as product gases away from the catalyst. Thus, high water diffusivity and gas permeability are required. As a result, a more porous binder material could improve the kinetics of mass transport at the reaction sites and thereby enhance the overall cell performance. In addition, in water electrolysers without supporting electrolyte sufficiently high hydroxide conductivities are crucial, too. An optimal water uptake (WU) facilitates ion-transport in the polymeric material, whereas excessive WU leads to excessive swelling and loss of mechanical strength, possibly followed by delamination of the MEA and leaching of catalyst particles.[18] WU and swelling ratio (SR) were determined as a function of temperature and *m*-TP/*p*-TP ratio (Fig. 1). As the ketone feed ratio was kept constant for all polymers, the ion-exchange capacity (IEC) was considered to be well comparable among the different materials (see Table 1). However, because of slight differences between the IEC values, the hydration number (λ) of each polymer was calculated and chosen for comparison. As expected, λ and SR increased with increasing temperature for both the hydroxide and the chloride forms (Fig. 1a–d and S5†). Both forms were investigated to provide a comprehensive overview and enable comparison to the

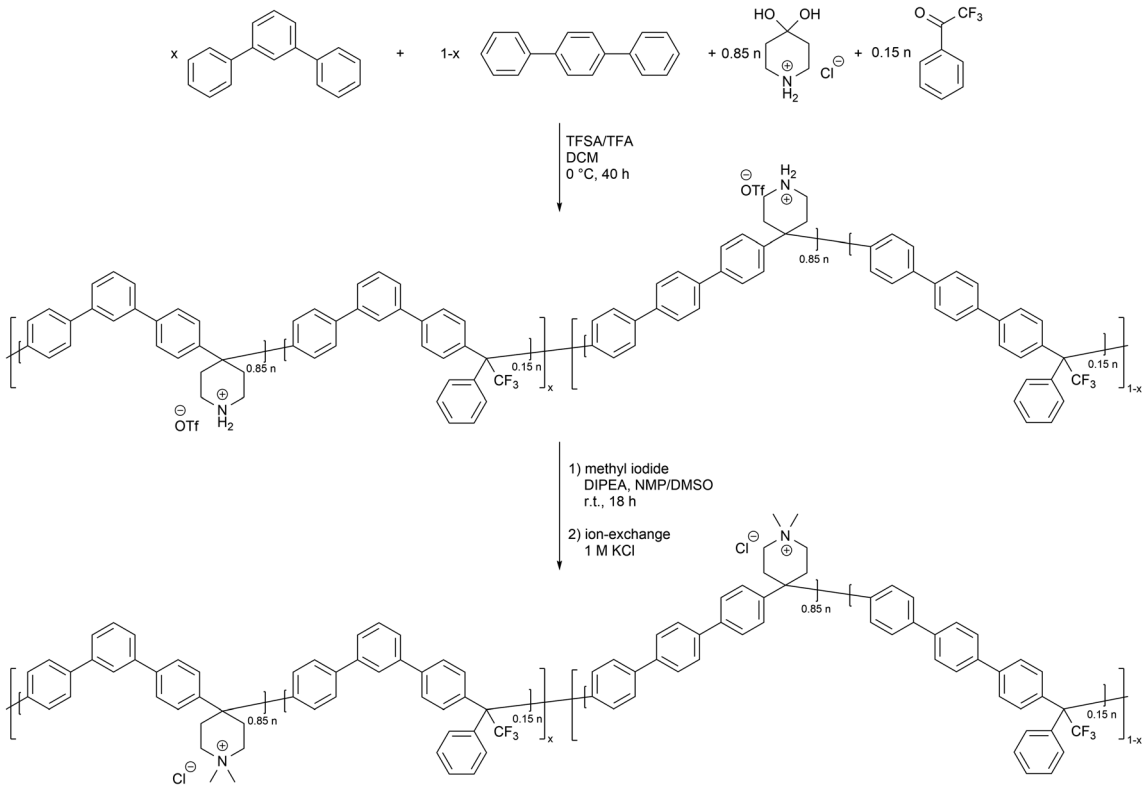

Scheme 1 Syntheses of ionomer binders with controlled *meta*-kinks *via* polyhydroxyalkylation (TFSA: trifluoromethanesulfonic acid, DIPEA: *N*,*N*-diisopropylethylamine, NMP: *N*-methylpyrrolidone, DMSO: dimethylsulfoxide).

literature where often one form is investigated only. When comparing the polymers with each other there is a clear trend that the gradual introduction of *meta*-kinks in the polymer backbones causes a gradual increase in λ and SR (Fig. 1 and S5†). For example, M0 has a hydration number of 14.4 at 80 °C in hydroxide and 9.3 at 90 °C in chloride form whereas the values for M100 are 32.2 and 11.6, respectively (Fig. 1c and S5b†). We explain this trend by a decreased backbone rigidity for increasing *meta*-kinks in the polymer main-chain, leading to increasing water uptake. The slopes of the regression lines of Fig. 1d become steeper with increasing temperature. This is interpreted as a higher temperature dependency of the water uptake the more *meta*-kinks are introduced in the polymer main-chain. The same trend is also seen in Fig. 1c where M100 shows a large increase in λ from 60 to 80 °C not observed for the other polymers, which arises from the more kinked and flexible backbone of M100.

The swelling of the materials was determined by measuring the dimensional changes after immersion in water and equilibration at several temperatures (Fig. 1a, b and S5a†). First, swelling of the chloride forms of all polymers is significantly lower than of the hydroxide forms, in agreement with the trends of the corresponding hydration numbers. Second, with increasing *m*-TP content, the dimensional swelling increased as well. For example, M0 shows a through-plane SR of 36% and an in-plane (areal) SR of 33% at 80 °C, whereas M100 gives values of 52% and 42%, respectively. This observation is again in agreement with the observed trends of hydration numbers and arises from the more kinked backbone when *meta*-terphenyl units are introduced. We hypothesize that such behaviour

Table 1 Molar masses, dispersity and ion exchange capacity (IEC) values of the investigated ionomers

Polymer	*m*-TP/*p*-TP feed ratio	$\bar{M}_n$ (kg mol^{-1})	$\bar{M}_w$ (kg mol^{-1})	$Đ$	IEC(Cl^-) (meq. g^{-1})	IEC(OH^-) (meq. g^{-1})	BET surface area (m^2 g^{-1})
M100	100/0	74.4	191.1	2.6	2.17	2.26	31.8
M85	85/15	19.6	51.5	2.6	2.16	2.25	
M65	65/35	25.7	67.3	2.6	2.15	2.25	
M50	50/50	25.6	71.8	2.8	2.14	2.23	24.0
M35	35/65	34.8	70.5	2.0	2.13	2.22	
M15	15/85	29.1	74.3	2.6	2.18	2.28	
M0	0/100	27.8	65.2	2.3	2.19	2.28	15.5

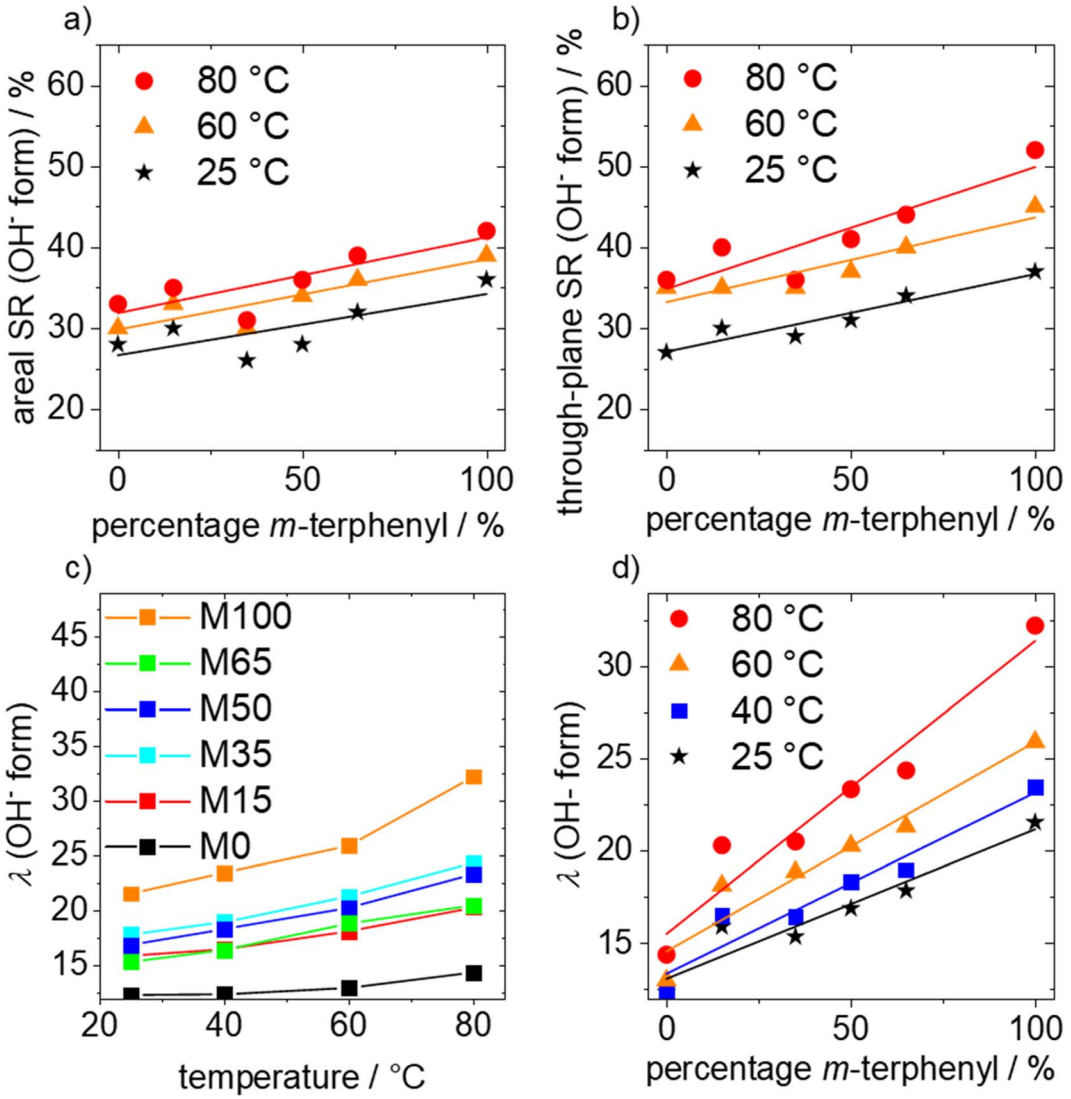

Fig. 1 Swelling ratios (a and b) and hydration numbers (c and d) of the hydroxide forms of M*x*.

correlates with changes in free volume, and thus nano/micro-porosity.[64] To confirm this hypothesis, specific surface areas were determined using the Brunauer Emmett Teller (BET) method (Table 1, for adsorption isotherms see Fig. S6†). The comparison of M100 and M0 with exclusive *meta*-terphenyl and *para*-terphenyl as the aryl monomer, respectively, clearly confirms a double specific surface area of the polymer M100 with only *meta*-kinked arylene units in the backbone. Such enhanced porosity is expected to facilitate gas permeability of products formed during the oxygen evolution reaction. Additionally, it can be derived from Table 1 that the introduction of *meta*-terphenyl in the polymer structures leads to a significantly high increase of the BET surface area. This could be explained by the lower probability for dense packing in the presence of a more kinked backbone structure. Finally, we note that in-plane and through-plane swelling of the hydroxide forms are of the same order of magnitude hinting at structurally isotropic membranes.

Ionic conductivity

The in-plane conductivities under immersed conditions of the prepared ionomers in chloride (Fig. S7†) and hydroxide forms (Fig. 2) where determined using a four-probe measurement cell in deionized water at different temperatures.[65] In addition, chloride-conductivities were determined in-plane at different temperatures and under a relative humidity of 95%, using a four-point probe geometry. Trends comparable to those under immersed conditions were obtained (Fig. S8†). Fig. S7a† shows the chloride conductivities and their temperature-dependent behaviour. The conductivity increases with increasing temperature due to the higher mobility of chloride ions. All polymers feature an Arrhenius-like behaviour (Fig. S7b†), with activation energies ranging from 23.1 to 26.2 kJ mol^{-1}. Furthermore, similar to changes in WU and SR with increasing *m*-TP units, also the conductivity increases from 84.5 to 110.8 mS cm^{-1} for M0 to M100, respectively. We ascribe the higher ion

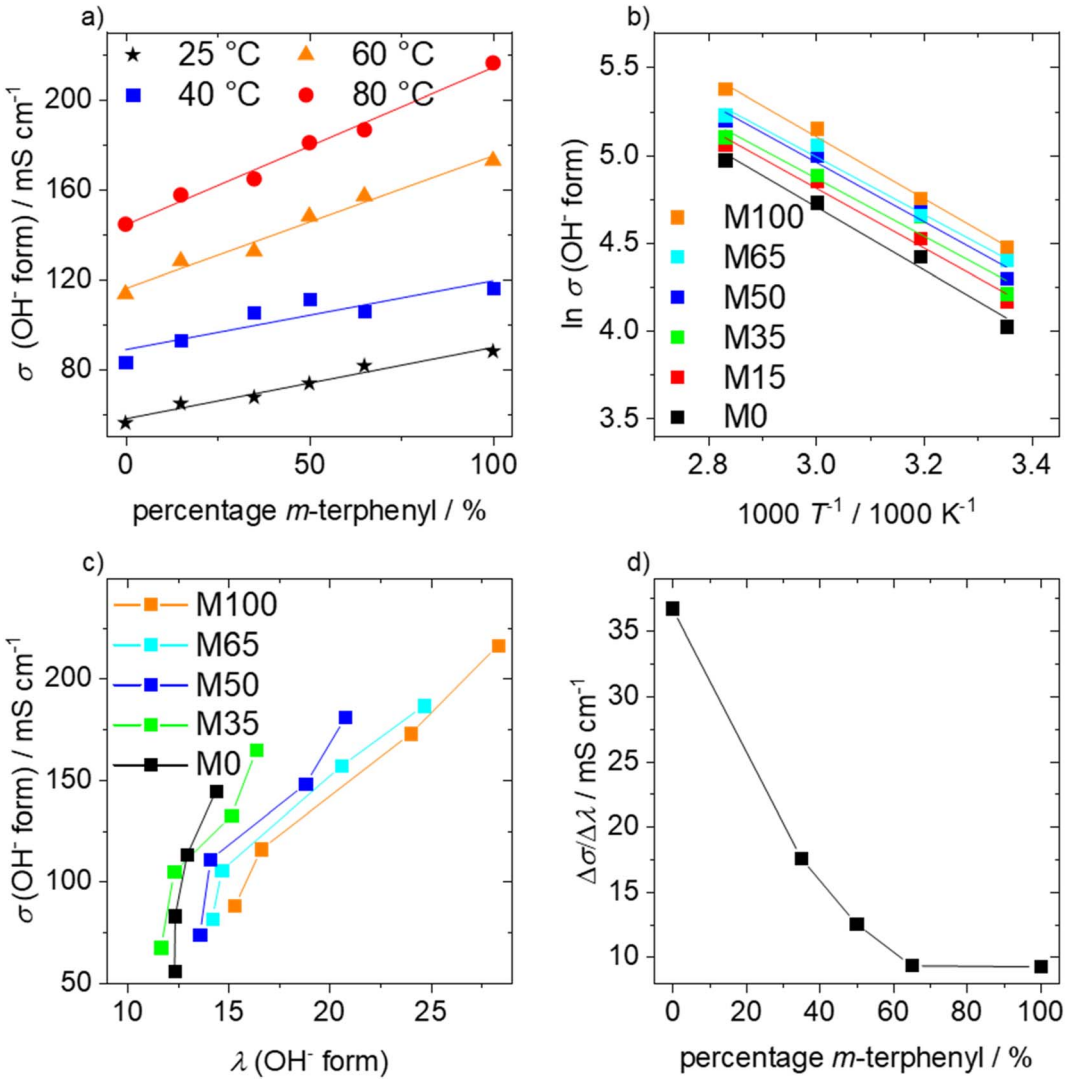

Fig. 2 Hydroxide conductivities of M*x* depending on the number of *meta*-kinks (a) and Arrhenius plots (b). Hydroxide conductivities depending on the hydration number (c) and the corresponding slopes depending on the percentage *m*-terphenyl in the polymers (d).

conductivity of more kinked ionomers to the higher water content (λ) and swelling leading to increased ion mobility.

In Fig. S7c† chloride conductivities at variable temperatures depending on the related hydration numbers of selected polymers are shown. In Fig. S7d,† the slopes of Fig. S7c† are shown which decrease for increasing *m*-TP units. These two plots suggest that polymers with more *meta*-kinks in the main-chain are less efficient ion-conductors regardless of their individual IEC and overall measured conductivity value, meaning that lower ion conductivities are obtained for a certain hydration state.[40,49,66]

Conductivities of the hydroxide forms are presented in Fig. 2.[65,67] Values range between 144.6 to 216.4 mS cm^{-1} at 80 °C which is in accordance with literature.[48] Conductivities correlate with the temperature- and *meta*-kink-dependent trends of the WU (Fig. 2a). A higher ion-mobility compared to the chloride form is indicated by the lower activation energies between 14.1 and 15.7 kJ mol^{-1} (Fig. 2b) which are in the range of previously reported poly(arylene piperidinium)s.[50,52] As for the chloride forms, the more *meta*-kinks present in the polymer backbone, the higher the hydration of the ionomers. Nevertheless, as observed for the chloride forms, the ion conductivity depending on a certain hydration state decreases with increasing *meta*-kinks (Fig. 2c). Fig. 2d shows the slopes of Fig. 2c which are decreasing with increasing fraction of *meta*-terphenyl, hinting at a less efficient ionic conductivity with increasing content of *meta*-kinks. Thus, the trends of hydroxide and chloride conductivities match well and indicate that, when focussing on high values for ion conductivity without increasing the IEC, the introduction of *meta*-kinks is a suitable strategy, even though the increase is caused by the higher WU.

Thermal stability and mechanical properties

The thermal stabilities of the AEM polymers were determined using thermogravimetric analysis (TGA, Fig. S9†). Thermal stabilities were evaluated by the decomposition temperature at

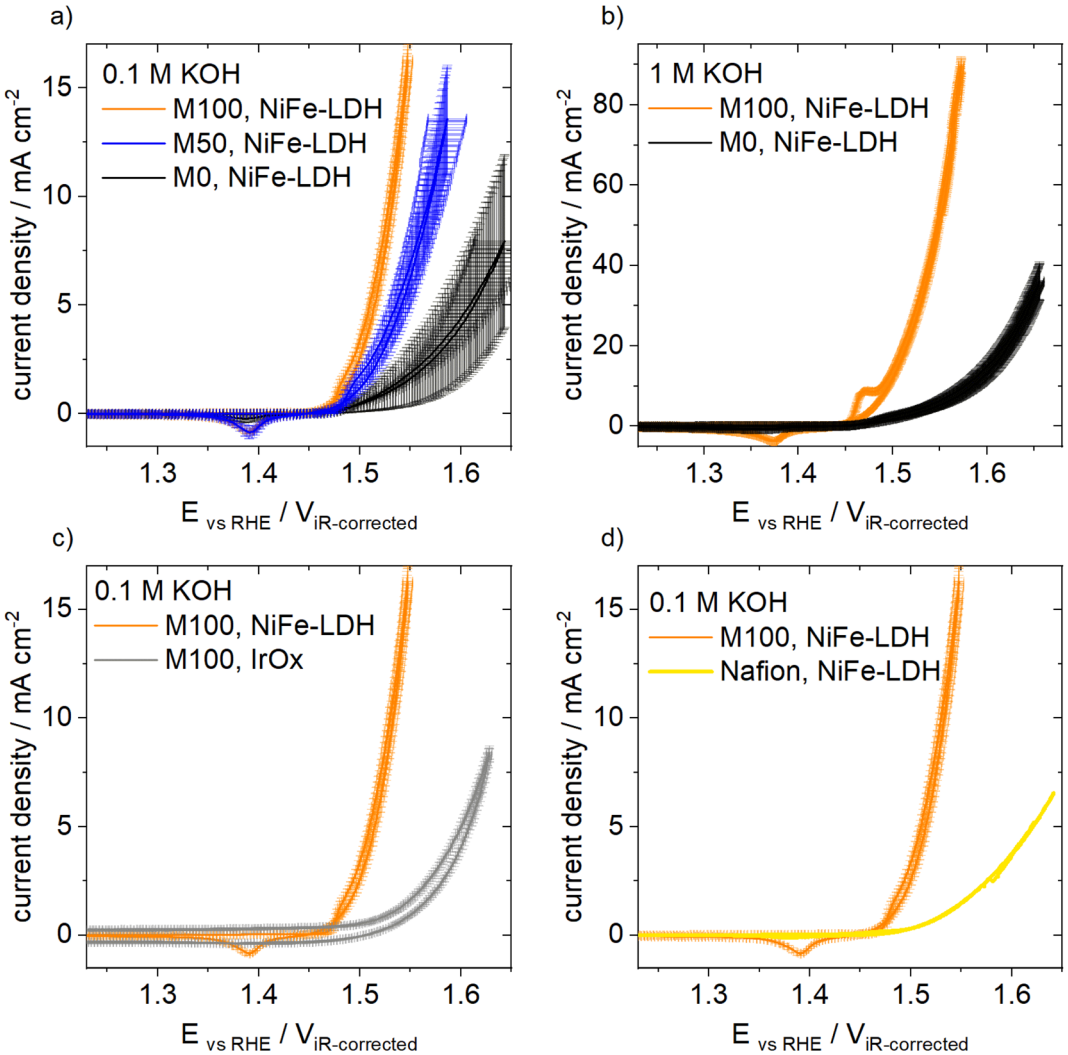

Fig. 3 (a) OER activities for differently kinked binder polymers in RDE with NiFe-LDH catalyst in 0.1 M KOH solution. OER activities for differently kinked binder polymers in RDE with NiFe-LDH catalyst in 0.1 M (a) and 1 M KOH solution (b) including error bars. Comparison of OER activities using either NiFe-LDH or IrOx as catalyst and M100 as binder polymer (c) and using either M100 or Nafion as binder polymer and NiFe-LDH as catalyst (d).

95% weight ($T_{d,95}$). All synthesized polymers showed sufficiently high $T_{d,95}$ values ranging from 266 to 303 °C, making them suitable for AEMWE under working conditions. The thermal decomposition of all polymers proceeded within three steps: At approximately 250 °C the quaternary ammonium units might be degraded, followed by side-chain cleavage at ~370 °C. Ultimately, decomposition of the aromatic polymer backbone begins at 500 °C in agreement with reported values.[68,69] Apart from this behaviour, significant differences between differently kinked polymers were absent.

To assess the mechanical integrity of the investigated polymers stress–strain experiments were conducted. Dumbbell-shaped specimens were cut from the membranes and studied as dry chloride forms under ambient conditions. We note that such conditions are far from those of AEMWE working conditions, but nevertheless allow to map relative differences among the samples. As shown in Fig. S10,† all polymers reach tensile strengths (T_s) of about 50 MPa with elongations at break (E_b) of at least 30%. Apart from M100, significant differences in ductility were not observed. This observation could be attributed to the incorporation of the stiff *para*-terphenylene unit in all of these polymers. In the case of only *meta*-terphenyl as an aryl monomer, ductility drastically increased because there are only kinked *meta*- and sp^3-carbons in the polymer backbone and the associated increased free volume. The larger molar mass of M100 compared to all other polymers likely contributes to the strong increase in E_b (108% for M100).

Binder performance from rotating disk electrode (RDE) measurements

The polymers were investigated as binders for catalysts in the oxygen evolution reaction (OER) using rotating disk electrode (RDE) experiments (Fig. 3). Disk electrodes were prepared from different catalysts and M0, M50 and M100 as binders. Nafion

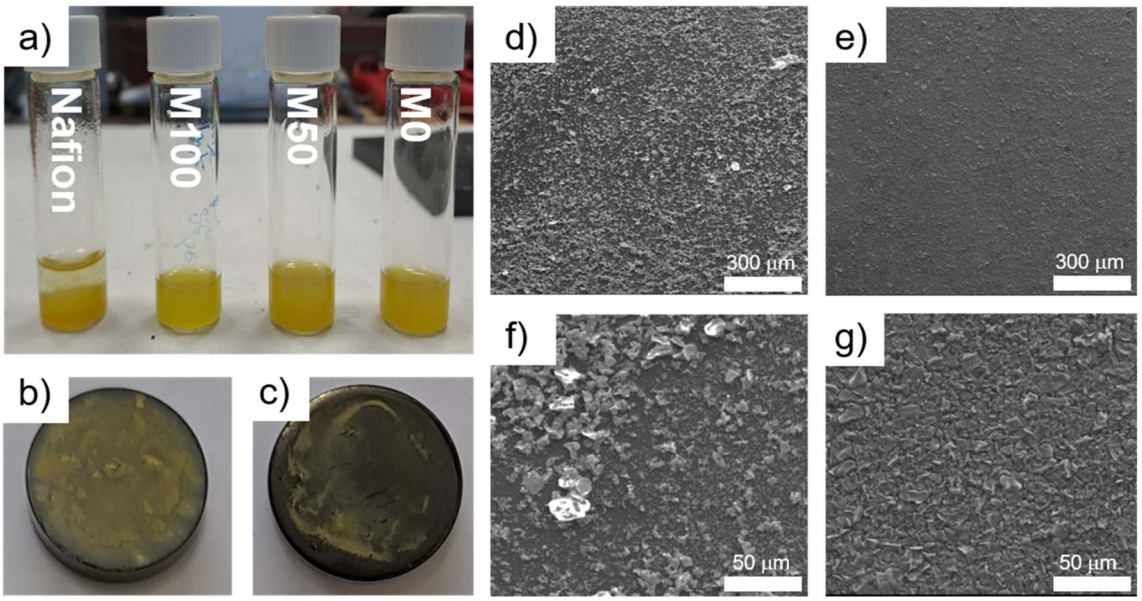

Fig. 4 (a) Catalyst ink dispersions prepared with different binders. Photographs of the electrodes coated with (b) NiFe-LDH/Nafion and (c) NiFe-LDH/PAP. SEM images of the surface of the electrodes with different magnification with Nafion (d and f) and M100 (e and g) as binder.

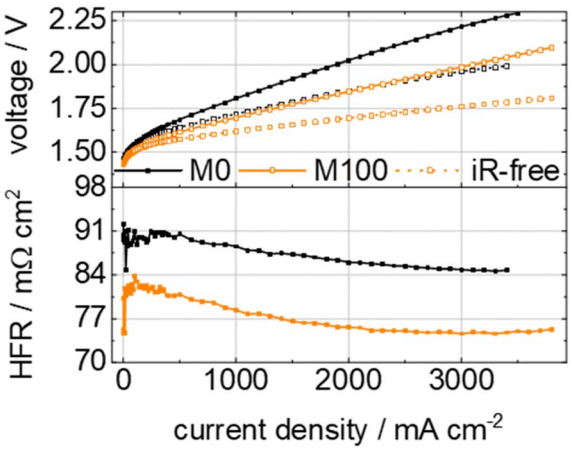

Fig. 5 Polarization curves and high-frequency resistance extracted from electrochemical impedance spectroscopy for 1 M KOH-fed operation in an AEM water electrolyser at 60 °C.

was used in addition as a commercial reference and literature-known binder for RDE-assisted catalyst characterization.[70] The RDE measurements were conducted in 0.1 M and 1 M KOH solution at room temperature and a rotation rate of 1600 rpm. As one of the greatest strengths of AEMWE is the possibility to use non-precious metal catalysts, NiFe-LDH was employed.

As seen in Fig. 3a and b the onset of current density increases at lower potential and with a larger slope with increasing content of *meta*-kinks. This trend is explained by enhanced hydration and the resulting improved ion transport. Since the investigated electrode reaction produces a gaseous product, gas permeability is also an important property. Additionally, the stability of these electrodes over 2000 cycles was investigated (Fig. S11b and S10d†). While the current density of the electrode made from M100 (Fig. S11b†) remained in the same range after testing, M50 (Fig. S11c†) and M0 (Fig. S11d†) delivered increasingly smaller values. For an example of Nyquist plots see Fig. S12.† The decrease in stability during RDE testing is explained by the formation of microbubbles on the surface of the electrode, limiting the escape of oxygen from the catalytically active sites.[71] Accordingly, the active area is reduced and the electrochemical reaction is slowed down. We correlate the superior binder performance of M100 in RDE experiments with the high content of *m*-TP-kinks causing a higher nanoporosity, larger WU and higher conductivity compared to M50 and M0. Furthermore, the increasing error bars for decreasing *meta*-terphenyl content in Fig. 3a might also hint at a decreasing binding capability, inferior surface homogeneity and non-optimal interaction of binder and NiFe-LDH catalyst.

Additional RDE experiments were carried out to compare M100 as binder for NiFe-LDH and iridium oxide (IrOx) as catalysts (Fig. 3c). Strikingly, the combination of M100 and NiFe-LDH delivered the best performance, which even outperformed the electrode prepared from the established and highly active IrOx. Notably, using M100 as a binder for IrOx appears to be a rather inefficient combination. Further confirmation of the exceptional performance of M100 as binder in RDE experiments was obtained by using Nafion as commercial binder ionomer (Fig. 3d), with M100 delivering a strongly improved overall performance. This observation indicates more efficient gas removal from the catalyst surface, which is explained by the surface morphologies of the RDE featuring a homogeneous distribution of catalyst particles (*vide supra*).

Fig. 4 shows compatibility and morphological aspects of binder catalyst combinations. Fig. 4a depicts NiFe-LDH ink dispersions with different ionomer binders, demonstrating Nafion dispersions to be unstable compared to PAP. This lead to

differences in homogeneities of RDE surfaces (Fig. 4b and c). To further visualize the impact of dispersion quality and ink stability on the surface morphology of RDEs, scanning electrode microscopy (SEM) was employed (Fig. 4d and e). Compared to the Nafion-based electrode (Fig. 4d), the use of M100 as binder enabled a more homogeneous distribution of catalyst particles (Fig. 4e), resulting in a more efficient catalyst utilization and consequently, a higher electrochemically active surface area as well as a more porous layer with less agglomerates.

AEMWE single cell performance

Finally, the performance of M100 and M0 as binders for membrane electrode assemblies (MEAs) used for AEM water electrolysis was evaluated (Fig. 5). The PAP ionomers were applied in the NiFe-LDH anodes of the MEAs. Catalyst-coated membranes (CCMs) were fabricated by direct deposition of the catalyst ink onto a 50 μm monolithic Aemion+ membrane as reported previously.[61] For both CCMs a previously established Pt/C cathode was used. In literature, only PAP ionomers resembling M0 have been used as binder, as they are commercially available as PiperION by Versogen.[15,72] To the best of our knowledge, despite numerous indications of increasing free volume when introducing *meta*- kinks[38,40,73] in the polymer main chain and the accompanying increase in porosity, studies applying *meta*-terphenyl (or otherwise kinked units) containing PAP as AEMWE binders are barely conducted.[32,74]

Similar to the results of the RDE, the cells with NiFe-LDH and with M100 as binder showed significantly lower overpotentials compared to the M0 analogs at 60 °C in 1 M KOH (Fig. 5). At 1.8 V, M100 and M0 delivered current densities of ~1700 mA cm^{-2} and 1000 cm^{-2}, respectively. This cannot be explained by the slightly higher high-frequency resistance (HFR) of the M0 cell alone, which amounts to 89 mΩ cm^2 at 1000 mA cm^{-2} compared to 78 mΩ cm^2 at 1000 mA cm^{-2} for M100. Also, the *iR*-free polarization curve showed lower voltages at all current densities. This indicates a higher NiFe-LDH activity in the MEA, potentially due to enhanced catalyst utilization which can be attributed to the higher available surface area of the more porous M100 (see BET surface areas, Table 1). In addition, the superior hydration and thus increased ion conductivity in combination with presumably higher gas permeability (as deduced from RDE) of the kinked M100 increase mass transport, which is of major importance for AEMWE operation.

Conclusions

We have conducted an in-depth study on the pristine properties of a series of poly(arylene piperidinium) ionomers with varying *meta*-terphenyl content along with their performance as binders in anion-exchange membrane water electrolysers (AEMWE). A series of seven PAP ionomers with varying *meta*- and *para*-terphenyl ratio but otherwise comparable properties were synthesized and comprehensively characterized with respect to water uptake, swelling ratio, porosity and ionic conductivity. All these properties follow the trend of a continuous increase with increasing *meta*-kink content. The central effect of *meta*-kinks in the polymer backbone is an increase in the specific surface area, leading to increased water uptake, which in turn affects all other properties associated with a higher degree of hydration. In addition, PAP ionomers turn out to be excellent binders for NiFe-LDH catalysts, probed by both rotating disk electrode measurements as well as AEMWE single cell performance. Here, an increasing content of *meta*-kinks is highly beneficial as well, for both binder dispersion and electrode quality as well as for gas permeation. The superior performance of fully *meta*-kinked PAP as anode binder matches well with the trends from RDE experiments. AEMWE single cells yield current densities of 1700 mA cm^{-2} at 1.8 V and 3000 mA cm^{-2} at 2.0 V, which are among the highest values obtained at 60 °C for state-of-the-art AEMWE cells.[3,32,75,76] In summary, this work emphasizes the importance of individual AEMWE binder optimization next to membrane development, with the former being a much less investigated aspect of AEMWE research.

Author contributions

Richard Weber: investigation, methodology, validation, writing – original draft. Malte Klingenhof: investigation, methodology, validation, writing – review & editing. Susanne Koch: investigation, methodology, validation, writing – review & editing. Lukas Metzler: investigation, methodology, validation, writing – review & editing. Thomas Merzdorf: investigation, methodology, Jochen Meier-Haack: investigation, methodology, validation. Severin Vierrath: conceptualization, funding acquisition, supervision. Peter Strasser: conceptualization, funding acquisition, supervision. Michael Sommer: conceptualization, funding acquisition, supervision, writing – review & editing.

Conflicts of interest

There are no conflicts to declare.

Acknowledgements

The authors thank Hannes Nederstedt for help in establishing ion conductivity measurements, Rukiya Matsidik for BET measurements, Luis Hagner for measuring one of the AEMWE cells and Patricia Godermajer for TGA measurements. Funding from the BMBF (AEMready, Grant No. 03SF0613A) is greatly acknowledged.

References

1 H. A. Miller, K. Bouzek, J. Hnat, S. Loos, C. I. Bernäcker, T. Weißgärber, L. Röntzsch and J. Meier-Haack, *Sustainable Energy Fuels*, 2020, **4**, 2114–2133.
2 K. Ayers, N. Danilovic, R. Ouimet, M. Carmo, B. Pivovar and M. Bornstein, *Annu. Rev. Chem. Biomol. Eng.*, 2019, **10**, 219–239.

3 D. Li, A. R. Motz, C. Bae, C. Fujimoto, G. Yang, F.-Y. Zhang, K. E. Ayers and Y. S. Kim, *Energy Environ. Sci.*, 2021, **14**, 3393–3419.
4 A. Buttler and H. Spliethoff, *Renewable Sustainable Energy Rev.*, 2018, **82**, 2440–2454.
5 P. Shirvanian, A. Loh, S. Sluijter and X. Li, *Electrochem. Commun.*, 2021, **132**, 107140.
6 C. Huang, Q. Zhou, D. Duan, L. Yu, W. Zhang, Z. Wang, J. Liu, B. Peng, P. An, J. Zhang, L. Li, J. Yu and Y. Yu, *Energy Environ. Sci.*, 2022, **15**, 4647–4658.
7 M. Xiao, C. Wu, J. Zhu, C. Zhang, Y. Li, J. Lyu, W. Zeng, H. Li, L. Chen and S. Mu, *Nano Res.*, 2023, **16**, 8945–8952.
8 A. Y. Faid and S. Sunde, *Energy Technol.*, 2022, **10**, 2200506.
9 R. Abbasi, B. P. Setzler, S. Lin, J. Wang, Y. Zhao, H. Xu, B. Pivovar, B. Tian, X. Chen, G. Wu and Y. Yan, *Adv. Mater.*, 2019, **31**, 1805876.
10 D. S. Kim, C. Welch, R. P. Hjelm, Y. S. Kim and M. D. Guiver, in *Polymer Science: A Comprehensive Reference*, ed. K. Matyjaszewski and M. Möller, Elsevier, Amsterdam, 2012, pp. 691–720.
11 N. Du, C. Roy, R. Peach, M. Turnbull, S. Thiele and C. Bock, *Chem. Rev.*, 2022, **122**, 11830–11895.
12 N. Chen and Y. M. Lee, *Prog. Polym. Sci.*, 2021, **113**, 101345.
13 S. Holdcroft, *Chem. Mater.*, 2014, **26**, 381–393.
14 B. Mayerhöfer, K. Ehelebe, F. D. Speck, M. Bierling, J. Bender, J. A. Kerres, K. J. J. Mayrhofer, S. Cherevko, R. Peach and S. Thiele, *J. Mater. Chem. A*, 2021, **9**, 14285–14295.
15 G. A. Lindquist, S. Z. Oener, R. Krivina, A. R. Motz, A. Keane, C. Capuano, K. E. Ayers and S. W. Boettcher, *ACS Appl. Mater. Interfaces*, 2021, **13**, 51917–51924.
16 W. You, K. J. T. Noonan and G. W. Coates, *Prog. Polym. Sci.*, 2020, **100**, 101177.
17 E. J. Park and Y. S. Kim, *J. Mater. Chem. A*, 2018, **6**, 15456–15477.
18 D. Li, A. R. Motz, C. Bae, C. Fujimoto, G. Yang, F.-Y. Zhang, K. E. Ayers and Y. S. Kim, *Energy Environ. Sci.*, 2021, **14**, 3393–3419.
19 A. R. Motz, D. Li, A. Keane, L. D. Manriquez, E. J. Park, S. Maurya, H. Chung, C. Fujimoto, J. Jeon, M. K. Pagels, C. Bae, K. E. Ayers and Y. S. Kim, *J. Mater. Chem. A*, 2021, **9**, 22670–22683.
20 R. A. Krivina, G. A. Lindquist, M. C. Yang, A. K. Cook, C. H. Hendon, A. R. Motz, C. Capuano, K. E. Ayers, J. E. Hutchison and S. W. Boettcher, *ACS Appl. Mater. Interfaces*, 2022, **14**, 18261–18274.
21 I. Wu, K. C. Dunn, J. W. Creel, A. N. Radzanowski, K. J. Beiler, M. S. Ezell, A. M. Johnson, D. J. Carmosino, M. J. Salgado, C. Kim, M.-C. Kuo, N. C. Buggy, S. Seifert, E. B. Coughlin and A. M. Herring, *ACS Appl. Polym. Mater.*, 2023, **5**, 5834–5845.
22 J. H. Hsu, C. R. Peltier, M. Treichel, J. C. Gaitor, Q. Li, R. Girbau, A. J. Macbeth, H. D. Abruña, K. J. T. Noonan, G. W. Coates and B. P. Fors, *Angew. Chem., Int. Ed.*, 2023, **62**, e202304778.
23 D. Li, E. J. Park, W. Zhu, Q. Shi, Y. Zhou, H. Tian, Y. Lin, A. Serov, B. Zulevi, E. D. Baca, C. Fujimoto, H. T. Chung and Y. S. Kim, *Nat. Energy*, 2020, **5**, 378–385.
24 L. Xiao, S. Zhang, J. Pan, C. Yang, M. He, L. Zhuang and J. Lu, *Energy Environ. Sci.*, 2012, **5**, 7869–7871.
25 J. Pan, Y. Li, L. Zhuang and J. Lu, *Chem. Commun.*, 2010, **46**, 8597–8599.
26 J. Parrondo, C. G. Arges, M. Niedzwiecki, E. B. Anderson, K. E. Ayers and V. Ramani, *RSC Adv.*, 2014, **4**, 9875–9879.
27 Y. Leng, G. Chen, A. J. Mendoza, T. B. Tighe, M. A. Hickner and C.-Y. Wang, *J. Am. Chem. Soc.*, 2012, **134**, 9054–9057.
28 C. Busacca, S. C. Zignani, A. Di Blasi, O. Di Blasi, M. Lo Faro, V. Antonucci and A. S. Aricò, *Int. J. Hydrogen Energy*, 2019, **44**, 20987–20996.
29 D. Xu, M. B. Stevens, M. R. Cosby, S. Z. Oener, A. M. Smith, L. J. Enman, K. E. Ayers, C. B. Capuano, J. N. Renner, N. Danilovic, Y. Li, H. Wang, Q. Zhang and S. W. Boettcher, *ACS Catal.*, 2019, **9**, 7–15.
30 S. Koch, P. A. Heizmann, S. K. Kilian, B. Britton, S. Holdcroft, M. Breitwieser and S. Vierrath, *J. Mater. Chem. A*, 2021, **9**, 15744–15754.
31 B. Chen, P. Mardle and S. Holdcroft, *J. Power Sources*, 2022, **550**, 232134.
32 N. Chen, S. Yane Paek, J. Yeon Lee, J. Hyeong Park, S. Young Lee and Y. Moo Lee, *Energy Environ. Sci.*, 2021, **14**, 6338–6348.
33 H. Koshikawa, H. Murase, T. Hayashi, K. Nakajima, H. Mashiko, S. Shiraishi and Y. Tsuji, *ACS Catal.*, 2020, **10**, 1886–1893.
34 D. Chanda, J. Hnát, T. Bystron, M. Paidar and K. Bouzek, *J. Power Sources*, 2017, **347**, 247–258.
35 D. Chanda and S. Basu, *Int. J. Hydrogen Energy*, 2018, **43**, 21999–22011.
36 R. A. Tufa, E. Rugiero, D. Chanda, J. Hnàt, W. van Baak, J. Veerman, E. Fontananova, G. Di Profio, E. Drioli, K. Bouzek and E. Curcio, *J. Membr. Sci.*, 2016, **514**, 155–164.
37 W.-H. Lee, Y. S. Kim and C. Bae, *ACS Macro Lett.*, 2015, **4**, 814–818.
38 W.-H. Lee, E. J. Park, J. Han, D. W. Shin, Y. S. Kim and C. Bae, *ACS Macro Lett.*, 2017, **6**, 566–570.
39 E. J. Park, C. B. Capuano, K. E. Ayers and C. Bae, *J. Power Sources*, 2018, **375**, 367–372.
40 T. H. Pham, J. S. Olsson and P. Jannasch, *J. Mater. Chem. A*, 2019, **7**, 15895–15906.
41 T. Zhao, C. Long, Z. Wang and H. Zhu, *ACS Appl. Energy Mater.*, 2021, **4**, 14476–14487.
42 X. Zhou, L. Wu, G. Zhang, R. Li, X. Hu, X. Chang, Y. Shen, L. Liu and N. Li, *J. Membr. Sci.*, 2021, **631**, 119335.
43 S. Zhang, X. Zhu and C. Jin, *J. Mater. Chem. A*, 2019, **7**, 6883–6893.
44 D. Pan, S. Chen and P. Jannasch, *ACS Macro Lett.*, 2022, 20–25.
45 Q. Wang, L. Huang, Z. Wang, J. Zheng, Q. Zhang, G. Qin, S. Li and S. Zhang, *Macromolecules*, 2022, **55**, 10713–10722.
46 J. S. Olsson, T. H. Pham and P. Jannasch, *Adv. Funct. Mater.*, 2018, **28**, 1702758.

47 N. Chen, C. Lu, Y. Li, C. Long and H. Zhu, *J. Membr. Sci.*, 2019, **572**, 246–254.
48 J. Wang, Y. Zhao, B. P. Setzler, S. Rojas-Carbonell, C. B. Yehuda, A. Amel, M. Page, L. Wang, K. Hu, L. Shi, S. Gottesfeld, B. Xu and Y. Yan, *Nat. Energy*, 2019, **4**, 392–398.
49 J. S. Olsson, T. H. Pham and P. Jannasch, *J. Membr. Sci.*, 2019, **578**, 183–195.
50 L. Xu, H. Wang, L. Min, W. Xu, Y. Wang and W. Zhang, *Ind. Eng. Chem. Res.*, 2022, **61**, 14232–14241.
51 F. Wang, C. Li, J. Sang and J. Li, *Energy Fuels*, 2022, **36**, 7795–7805.
52 C. Long, Z. Wang and H. Zhu, *Int. J. Hydrogen Energy*, 2021, **46**, 18524–18533.
53 X. Wang, C. Lin, Y. Gao and R. G. H. Lammertink, *J. Membr. Sci.*, 2021, **635**, 119525.
54 R. Ma, Y. Kang, T. Wang, T. Jiang, H. Yin, C. Liu, H. Wei and Y. Ding, *J. Membr. Sci.*, 2023, 121667.
55 C. Fujimoto, D.-S. Kim, M. Hibbs, D. Wrobleski and Y. S. Kim, *J. Membr. Sci.*, 2012, **423–424**, 438–449.
56 Y.-K. Choe, C. Fujimoto, K.-S. Lee, L. T. Dalton, K. Ayers, N. J. Henson and Y. S. Kim, *Chem. Mater.*, 2014, **26**, 5675–5682.
57 A. Amel, L. Zhu, M. Hickner and Y. Ein-Eli, *J. Electrochem. Soc.*, 2014, **161**, F615.
58 C. G. Arges and V. Ramani, *Proc. Natl. Acad. Sci. U. S. A.*, 2013, **110**, 2490–2495.
59 S. Miyanishi and T. Yamaguchi, *Phys. Chem. Chem. Phys.*, 2016, **18**, 12009–12023.
60 A. D. Mohanty, S. E. Tignor, J. A. Krause, Y.-K. Choe and C. Bae, *Macromolecules*, 2016, **49**, 3361–3372.
61 S. Koch, L. Metzler, S. K. Kilian, P. A. Heizmann, F. Lombeck, M. Breitwieser and S. Vierrath, *Adv. Sustainable Syst.*, 2023, **7**, 2200332.
62 S. Koch, Doctoral thesis, Albert-Ludwigs-Universität Freiburg, 2023.
63 T. H. Pham, J. S. Olsson and P. Jannasch, *J. Mater. Chem. A*, 2018, **6**, 16537–16547.
64 S. A. Sydlik, Z. Chen and T. M. Swager, *Macromolecules*, 2011, **44**, 976–980.
65 N. Ziv and D. R. Dekel, *Electrochem. Commun.*, 2018, **88**, 109–113.
66 T. Jiang, C. Wu, Y. Zhou, S. Cheng, S. Yang, H. Wei, Y. Ding and Y. Wu, *J. Membr. Sci.*, 2022, **647**, 120342.
67 H. Khalid, M. Najibah, H. S. Park, C. Bae and D. Henkensmeier, *Membranes*, 2022, **12**, 989.
68 N. Chen, C. Lu, Y. Li, C. Long, Z. Li and H. Zhu, *J. Membr. Sci.*, 2019, **588**, 117120.
69 N. Chen, J. H. Park, C. Hu, H. H. Wang, H. M. Kim, N. Y. Kang and Y. M. Lee, *J. Mater. Chem. A*, 2022, **10**, 3678–3687.
70 E. Hornberger, M. Klingenhof, S. Polani, P. Paciok, A. Kormányos, R. Chattot, K. E. MacArthur, X. Wang, L. Pan, J. Drnec, S. Cherevko, M. Heggen, R. E. Dunin-Borkowski and P. Strasser, *Chem. Sci.*, 2022, **13**, 9295–9304.
71 H. A. El-Sayed, A. Weiß, L. F. Olbrich, G. P. Putro and H. A. Gasteiger, *J. Electrochem. Soc.*, 2019, **166**, F458–F464.
72 R. Rossi, R. Taylor and B. E. Logan, *ACS Sustain. Chem. Eng.*, 2023, **11**, 8573–8579.
73 D. Pan, P. M. Bakvand, T. H. Pham and P. Jannasch, *J. Mater. Chem. A*, 2022, **10**, 16478–16489.
74 X. Yan, X. Yang, X. Su, L. Gao, J. Zhao, L. Hu, M. Di, T. Li, X. Ruan and G. He, *J. Power Sources*, 2020, **480**, 228805.
75 D. Li, E. J. Park, W. Zhu, Q. Shi, Y. Zhou, H. Tian, Y. Lin, A. Serov, B. Zulevi, E. D. Baca, C. Fujimoto, H. T. Chung and Y. S. Kim, *Nat. Energy*, 2020, **5**, 378–385.
76 P. Fortin, T. Khoza, X. Cao, S. Y. Martinsen, A. Oyarce Barnett and S. Holdcroft, *J. Power Sources*, 2020, **451**, 227814.